Electron capture by fully stripped high-Z projectiles from the hydrogen atom

M. Das, N. C. Deb, N. C. Sil, and S. C. Mukherjee
Department of Theoretical Physics, Indian Association for the Cultivation of Science, Jadavpur, Calcutta 700 032, India
(Received 24 April 1995)

A single-channel distorted-wave approximation is used to calculate the one-electron capture cross section into an arbitrary state (nlm) of Ti^{22+}, V^{23+}, and Fe^{26+} from the ground state of a hydrogen atom. Since the interaction between the heavy projectile and the target electron is stronger, we represent the initial-channel wave function by a continuum distorted wave while the wave function in the final channel is taken to be a traveling atomic orbital. The nth partial cross sections are found to be in qualitative agreement with previous calculations for some other systems. It is found that at high energies the value $n_{\rm max}$, where the nth partial cross section is maximum, is larger by a few steps than obtained from the $n_{\rm max}=Z^{3/4}$ model. However, for a fixed projectile $n_{\rm max}$ moves towards the smaller values as the energy increases. The l dependence of the cross sections are also studied at different energies at the corresponding $n_{\rm max}$. We have further studied the mth partial cross sections at various energies and at the corresponding $n_{\rm max}$ for several l values. It is found that the contributions from higher m values are decreasing rapidly for $m>5$.

PACS number(s): 34.70.+e, 03.65.Nk, 32.80.Cy

I. INTRODUCTION

Ideally, fusion plasma should contain only hydrogen atoms and electrons. However, owing to the nonideal confinement of the high-temperature gas, energetic particles traverse the magnetic barriers and hit the walls of the limitors. As a result, wall particles are liberated which contaminate the plasma with impurity ions [1]. Inside the plasma charge-exchange reactions between these ions and neutral hydrogen atoms takes place, leading to enormous radiation losses [2,3]. Since it is not possible to avoid impurities altogether, much attention is given to finding methods to reduce the impurity concentration. A knowledge of various charge-exchange cross sections is needed to achieve this impurity control [4].

In the present investigation we therefore pick up some fully stripped impurity ions, e.g., Ti^{22+}, V^{23+}, and Fe^{26+}, and calculate the electron-capture cross sections by these ions from atomic hydrogen. As the projectile nuclear charge Z_P increases, the number of significant capture channels increases, and a quantum calculation for these processes becomes increasingly difficult. In the high-energy area, due to the large electron-momentum transfer effect these calculations become even more difficult. Ryufuku and Watanabe [5–7] used uniterized distorted-wave approximation (UDWA) and presented results for Si^{14+} up to 500 keV/amu and for Ca^{20+} up to 10 keV/amu. They also reported results for a few more projectiles of lower nuclear charges. For Si^{14+} they carried out calculations only up to $n_{\rm max}=12$, and accounted for the contributions corresponding to $n_{\rm max}>12$ channels by extrapolation. For Ca^{20+} they reported cross sections only up to $n=11$ and $E>10$ keV/amu. The results of Ryufuku and Watanabe [7] tend to overestimate above 100 keV/amu, as the authors themselves pointed out. Within the framework of eikonal approximation, Eichler [8] presented an analytic method for calculating nlm-$n'l'm'$ charge-transfer cross sections. But for high-Z projectiles ($Z=20$ and 25) they obtained the cross sections by using a simple scaling law developing earlier by Chan and Eichler [9,10]. Janev, Belkic, and Bransden [11] made a systematic investigation of the electron capture by projectiles of charges $Z=5$–74 from atomic hydrogen. They used a semiclassical multichannel Landau-Zener theory and presented total as well as partial cross sections (with respect to n and l) up to 80 keV/amu. However, this method is restricted for the transition to a product state with $n\geqslant Z$, although contributions to the total cross sections from such a product state would be small. Recently Toshima [12] reported capture cross sections by several fully stripped projectiles ($Z_P=2$–8) for low and intermediate energies. A few more calculations [13–15] are reported for similar collisional systems, mostly for the low-energy region; for the high-energy region the calculations are restricted to lower projectile charges.

In what follows, we shall study the following charge transfer processes:

$$A^{Z_P+}+\mathrm{H}(1s)\rightarrow A^{(Z_P-1)+}(nlm)+\mathrm{H}^+, \qquad (1)$$

where A^{Z_P+} represents fully stripped high Z_P projectiles such as Ti^{22+}, V^{23+}, and Fe^{26+}. Atomic units are used throughout the calculations.

II. THEORY

Under the usual continuum-distorted-wave (CDW) prescription of Crothers and Dunseath [16] the initial and final channel wave functions are given by

$$\begin{aligned} |\chi_i^{(+)}\rangle &= \phi_i(\vec{r}_T)\exp(i\vec{K}_i\cdot\vec{R}_T)N(\nu_p)\ {}_1F_1(i\nu_p;1;ivr_p+i\vec{v}\cdot\vec{r}_p),\\ |\xi^{(-)}\rangle &= \phi_f(\vec{r}_p)\exp(i\vec{K}_f\cdot\vec{R}_P)N^*(\nu_T)\ {}_1F_1(-i\nu_T;1;-ivr_T-i\vec{v}\cdot\vec{r}_T), \end{aligned} \qquad (2)$$

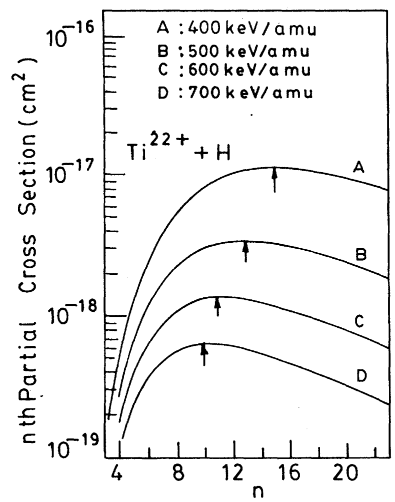

FIG. 1. nth partial cross sections (cm^2) as a function of n for electron capture by Ti^{22+} from the ground state of a hydrogen atom at several energies. A, 400 keV/amu; B, 500 keV/amu; C, 600 keV/amu; and D, 700 keV/amu.

where ϕ_i and ϕ_f are the bound states in the initial and final channels, respectively, and

$$\nu_i = Z_i/v, \quad N(\nu_i) = \exp(\tfrac{1}{2}\pi\nu_i)\Gamma(1-i\nu_i).$$

For the present one-electron transfer processes we ignore the nuclear-nuclear interaction V_{PT}. The stronger of the remaining two interactions V_p, i.e., the interaction between the bare projectile and the target electron, is taken through the Green's function G_p^+ and the wave function is obtained using the weaker interaction V_T between the target nucleus and the bound electron as the perturbative term. Then the first term of the distorted wave series is given by

$$T_{\mathrm{DW}}^{(-)} = \langle \xi_f^{(-)} | V_T | \chi_i^{(+)} \rangle . \tag{3}$$

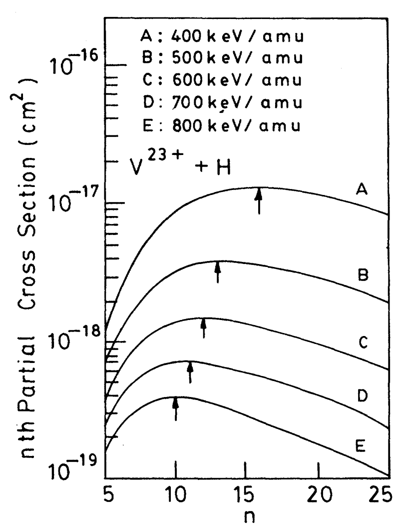

FIG. 2. Same as Fig. 1 for V^{23+} projectiles.

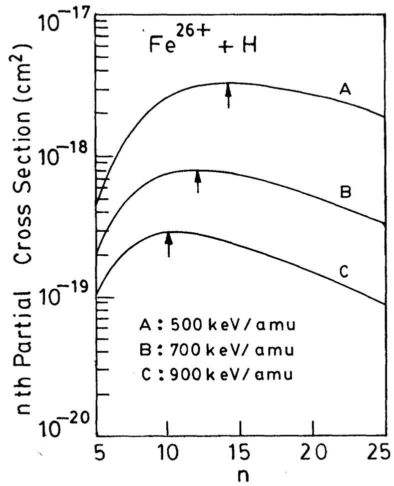

FIG. 3. Same as Fig. 1 for Fe^{26+} projectiles.

In CDW calculations, distortions in both channels are accounted for. But for high velocities and for very asymmetric collisions ($Z_P \gg Z_T$ in our case), a one-channel distorted-wave approximation is expected to provide a reasonable description of the collision mechanism. We take the final state as a traveling atomic orbital following

$$T_{\mathrm{DW}}^{(-)} = \langle \Psi_f | V_T | \chi_i^{(+)} \rangle , \tag{4}$$

where

$$|\Psi_f\rangle = \phi_f(\vec{r}_P)\exp(i\vec{K}_f\cdot\vec{R}_P),$$

and the initial state wave function $|\chi_i^{(+)}\rangle$ is given in Eq. (2).

A similar one-channel distorted-wave approximation, but for the reverse system ($Z_T \gg Z_P$), known as target continuum distorted wave (TCDW) approximation was developed earlier by Crothers and Dunseath [16] and generalized by Deb

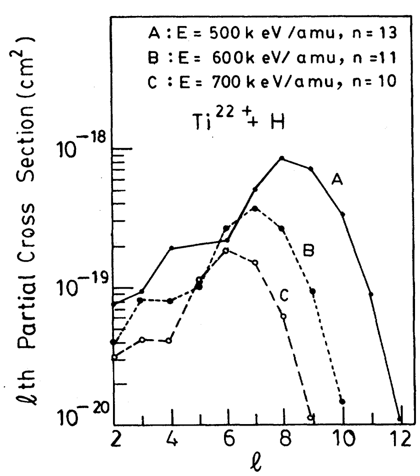

FIG. 4. lth partial cross sections (cm^2) as a function of l for Ti^{22+} projectiles at several energies. A, 500 keV/amu; B, 600 keV/amu; and C, 700 keV/amu.

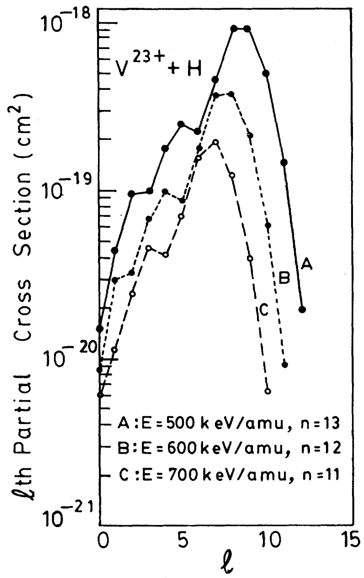

FIG. 5. Same as Fig. 4 for V^{23+} projectiles.

[17]. This approximation was then found to be suitable in several successive applications [16,18,19].

Transforming the coordinates $\vec{R}_P, \vec{R}_T$ to $\vec{r}_P, \vec{r}_T$, we then obtain

$$T_{\rm DW}^{(-)} = N(\nu_P) \int d r_T \phi_{1s}(\vec{r}_T) e^{i\vec{Q}\cdot\vec{r}_T} V_T(r_T)$$

$$\times \int d\vec{r}_P \phi_f^*(r_p) e^{-i\tilde{Q}\cdot\vec{r}_P}\ {}_1F_1(i\nu_P,1;i v r_P + i\vec{v}\cdot\vec{r}_P)$$

$$= N(\nu_P) I \tilde{I}, \tag{5a}$$

where

$$\mathbf{Q} = \vec{k}_i - \vec{k}_f - \tfrac{1}{2}\vec{v}, \quad \tilde{Q} = \vec{k}_i - \vec{k}_f + \tfrac{1}{2}\vec{v},$$

$$\vec{K}_i = \mu_P \vec{v}_i, \quad \vec{k}_i = \mu \vec{v}_i,$$

$$\vec{K}_f = \mu_T \vec{v}_f, \quad \vec{k}_f = \mu \vec{v}_f,$$

$$\mu_P = M_T(M_P+1)/M, \quad \mu_T = M_P(M_T+1)/M,$$

$$\mu = M_P M_T/(M_P+M_T), \quad M = M_T + M_P + 1.$$

The total cross section is then given by

$$\sigma = \frac{\mu_T \mu_P}{4\pi^2}(K_f/K_i) \int |T_{\rm DW}^{(-)}|^2 d\Omega. \tag{5b}$$

The integral I is evaluated to

$$I = 4(\pi Z_T^5)^{1/2}/(\lambda_i^2 + Q^2). \tag{6}$$

Following Deb [17] the integral $\tilde{I}$ can be evaluated as

$$\tilde{I} = 4\pi i^l A(n,l,\lambda_f) \sum_{k=0}^{n-l-1} B(n,l,k,\lambda_f) \sum_{r'=0}^{[(k+1)/2]} C(k,l,r') J_2, \tag{7}$$

where

$$J_2 = (2\pi i)^{-1} \int_\Gamma \frac{Q_1^l Y_{lm}^*(\hat{Q}_1) \lambda^N p(\nu_p, t) dt}{(\lambda^2 + Q_1^2)^M}, \tag{8a}$$

$$A(n,l,\lambda_f) = \left[(2\lambda_f)^3 \frac{(n-l-1)!}{2n[(n+l)!]^3} \right]^{1/2} (2\lambda_f)^l,$$

$$B(n,l,k,\lambda_f) = \frac{(-1)^{k+2l+1}[(n+l)!]^2}{(n-l-1-k)!(2l+1+k)!k!}(2\lambda_f)^k,$$

$$\lambda_f = Z_P/n,$$

$$C(k,l,r') = \frac{(-1)^{r'} 2^{k+l+1-2r'}(k+1)!(k+l+1-r')!}{(k+1-2r')!r'!},$$

$$\vec{Q}_1 = -\vec{\tilde{Q}} + \vec{v}t, \quad N = k+1-2r', \quad M = k+l+2-r',$$

$$\lambda = \lambda_f - i v t, \tag{8b}$$

and Γ is a closed contour encircling the points 0 and 1 once counterclockwise coming from the integral representation of the ${}_1F_1$ function appearing in Eq. (5).

TABLE I. mth partial cross sections (cm^2) for Ti^{22+} at 500 keV/amu ($n_{max}=13$) and at 700 keV/amu ($n_{max}=10$) for three l values making major contributions. $a\ [-b]$ stands for $a \times 10^{-b}$.

Case	l \ m	0	1	2	3	4	4
E=500 keV/amu	7	1.82[−19]	8.18[−20]	6.18[−20]	2.67[−20]	8.59[−21]	2.12[−21]
n=13	8	2.47[−19]	1.56[−19]	9.86[−20]	4.56[−20]	1.52[−20]	3.40[−21]
	9	1.90[−19]	1.42[−19]	8.82[−20]	4.28[−20]	1.56[−20]	4.56[−21]
E=700 keV/amu	5	5.12[−20]	1.84[−20]	8.53[−21]	2.77[−21]	3.69[−22]	7.25[−23]
n=10	6	6.95[−20]	3.72[−20]	1.65[−20]	5.45[−21]	1.29[−21]	2.57[−22]
	7	4.75[−20]	3.13[−20]	1.55[−20]	6.19[−21]	1.91[−21]	5.54[−22]

TABLE II. Same as Table I for V^{23+} projectiles.

Case	l \ m	0	1	2	3	4	5
$E=500$ keV/amu	8	21.63[−19]	6.16[−19]	1.07[−19]	5.21[−20]	1.80[−20]	4.09[−21]
$n=13$	9	2.40[−19]	1.78[−19]	1.13[−19]	5.60[−20]	2.09[−20]	6.08[−21]
	10	1.22[−19]	9.98[−20]	6.47[−20]	3.30[−20]	1.39[−20]	4.96[−21]
$E=700$ keV/amu	6	6.36[−20]	3.10[−20]	1.46[−20]	5.01[−21]	1.33[−21]	2.83[−22]
$n=10$	7	6.29[−20]	3.96[−20]	1.99[−20]	7.75[−21]	2.16[−21]	7.05[−22]
	8	3.40[−20]	2.50[−20]	1.36[−20]	6.04[−21]	2.27[−21]	8.26[−22]

Using the addition theorem [20,21] of regular solid harmonics, Deb [17] expanded $Q_1^l Y_{lm}(\hat{Q}_1)$ in terms of $Y_{lm}(\hat{k}_i)$ and $Y_{lm}(\hat{k}_f)$. This expansion will work for the s-s transition and/or for light particle scattering. But for a heavy particle collision where large momentum transfer is involved, expansion of $Q_1^l Y_{lm}(\hat{Q}_1)$ in terms of $Y_{lm}(\hat{k}_i)$ and $Y_{lm}(\hat{K}_f)$ will lead to serious numerical trouble. We therefore write

$$Q_1^l Y_{lm}^*(\hat{Q}_1)=\sum_{l'=0}^{l} N_{l'l''}t^{l'}, \tag{9a}$$

where

$$N_{l'l''}=\sum_{l'=0}^{l}\left[\frac{4\pi(2l+1)(l+m)!(l-m)!}{(2l'+1)(2l''+1)(l'+m')!(l'-m')!(l''+m'')!(l''-m'')!}\right]^{1/2}, \\ \times(-1)^{l''}v^{l'}Y_{l'm'}(\hat{v})\tilde{Q}^{l''}Y_{l''m''}(\hat{\tilde{Q}}),\quad l''=l-l',\quad m''=m-m'. \tag{9b}$$

Once again we closely follow the method of Deb [17] to obtain

$$\tilde{I}=4\pi i^l A(n,l,\lambda_f)\sum_{k=0}^{n-l-1}B(n,l,k,\lambda_f)\sum_{r'=0}^{[(k+1)/2]}C(k,l,r')\sum_{l'=0}^{l}N_{l'l''}\sum_{h=0}^{N}E(h,\lambda_f,v)\frac{(i\nu_P)_{l'+h}}{(l'+h)!}G^{-M}(1-H/G)^{1-M-i\nu_P} \\ \times {}_2F_1(1+l'+h-M;1-i\nu_P;l'+h+1;H/G), \tag{10a}$$

where

$$E(h,\lambda_f,v)=\frac{N!\lambda_f^{N-h}(-iv)^h}{h!(N-h)!},\quad G=\lambda_f^2+\tilde{Q}^2, \\ H=2i\lambda_f v+2\vec{\tilde{Q}}\cdot\vec{v}. \tag{10b}$$

For the present case $1+l'+h\leq M$, and hence the Gauss hypergeometric function in Eq. (10), will be a terminating series.

III. NUMERICAL TECHNIQUES AND RESULTS

As the projectile charge increases, the number of significant captured channels also increases. This makes a quantum calculation more and more difficult. As an example, for Fe^{26+} projectiles the contribution to the total cross section become significant even at $n=25$. For such a large n value, calculation of the functions like $A(n,l,\lambda_f)$, $B(n,l,k,\lambda_f)$, and $C(k,l,r')$ in Eq. (8b) poses a serious numerical difficulty due to the presence of large factorials such as $(n+l+1)$. We overcome this problem by calculating

$$\ln(n+l+1)!=\ln(n+l+1)+\ln(n+l)+\cdots+\ln 1.$$

This way, terms of the order of e^N will come down to N only. The equal order terms of the numerator and denominator of the above functions will cancel, and the result will come down to a small number. Values of the functions $A(n,l,\lambda_f)$, $B(n,l,k,\lambda_f)$, and $C(k,l,r')$ are then recovered accurately by taking the exponential of that small number.

As the relative velocity goes up, special care should be taken to calculate the v-dependent terms like G^{-M}, $(1-H/G)^{1-M-i\nu_P}$, $v^{l'}$, $\tilde{Q}^{l''}\ldots$, and their products. Sufficient analytic simplifications are needed before feeding into a computer for an accurate calculation of the cross sections, especially for the high velocities and large n values of the captured channels.

TABLE III. Same as Table I for Fe^{26+} projectiles.

Case	l \ m	0	1	2	3	4	5
E=500 keV/amu	8	1.56[−19]	7.19[−20]	6.28[−20]	3.67[−20]	1.55[−20]	3.51[−21]
n=13	9	2.30[−19]	1.56[−19]	1.10[−19]	6.09[−20]	2.44[−20]	7.28[−21]
	10	1.99[−19]	1.57[−19]	1.07[−19]	5.84[−20]	2.51[−20]	8.51[−21]
E=700 keV/amu	7	6.67[−20]	3.70[−20]	2.07[−20]	8.95[−21]	2.74[−21]	6.54[−22]
n=10	8	6.37[−20]	4.43[−20]	2.51[−20]	1.14[−20]	3.85[−21]	1.19[−21]
	9	3.41[−20]	2.68[−20]	1.61[−20]	7.74[−21]	3.23[−21]	1.18[−21]

To check our computer code we first run the code for Si^{14+} projectiles and compare our results with those of Ryufuku and Watanabe [5]. Our results are 5% above 100 keV/amu, but the general behavior of the nth partial cross sections is the same. For example, at 500 keV/amu we observe that $n_{max}=12$, which is in accordance with the findings of Ryufuku and Watanabe [5]. We then run our code for Ti^{22+}, V^{23+}, and Fe^{26+}, and present the nth partial cross sections (summed over all l and m values) as a function n at several energies in Figs. 1, 2, and 3, respectively. These figures show that n_{max} moves toward lower values as the energy goes up. For Ti^{22+} projectiles n_{max} moves down from 15 to 10 as the energy increases from 400 to 700 keV/amu; for V^{23+} projectiles these values move down from 16 to 10 as the energy goes up from 400 to 800 keV/amu; for Fe^{26+} projectiles these values move down from 14 to 10 as the energy increases from 500 to 900 keV/amu. From these three figures we observe that n_{max} has an energy dependence, and that movement of the n_{max} value gradually becomes slower as the energy goes up. This weak energy dependence of the n_{max} value was also observed by Janev, Belkic, and Bransden [11]. It is interesting to note that for 700-keV/amu Ti^{22+}, 800-keV/amu V^{23+}, and 900-keV/amu Fe^{26+} projectiles, n_{max} remains the same ($n_{max}=10$). At a fixed energy (keV/amu) varying the projectile charges from 22 to 26 (Ti^{22+} to Fe^{26+}), we see that n_{max} tends to increase very slowly. For example, at 500 keV/amu, n_{max} varies 13–14, whereas at 700 keV/amu it varies from 10 to 12 as the projectile charge moves from 22 to 26. The model $n_{max}=Z^{3/4}$ [7] agrees with our findings around 700 keV/amu. Below this energy the value of n_{max} is higher by a few steps than those obtained from this model.

We first select the n values for different energies at which the cross section is at a maximum (n_{max}), and plot the cross sections as a function of l corresponding to each of the n_{max} values in Figs. 4 and 5 corresponding to Ti^{22+} and V^{23+} projectiles, respectively. From Fig. 4 we find that the lth partial cross sections do not exhibit smooth behavior before reaching a sharp maximum l_{max} at $l=8$ for 500 keV/amu, $l=7$ for 600 keV/amu, and $l=6$ for 700 keV/amu. The cross sections fall off rapidly after reaching the maximum. In Fig. 5 we present the lth partial cross sections for V^{23+} at 500, 600, and 700 keV/amu. Unlike the case of Ti^{22+}, here the lth partial cross sections do not reach a single maximum at the first two energies (curves A and B) whereas at 700 keV/amu it does reach a single maximum (curve C). In all other aspects they are similar to those in Fig. 4.

We then study the m dependence of the cross sections for all the three projectiles, each at two energies. These values are tabulated in Tables I, II, and III, respectively. However, we present values for $m=0-5$ only, to show the slow variation of the cross sections as a function of m. After $m=5$ the values fall off rapidly. All these m values correspond to three different l values corresponding to $n=n_{max}$ at a particular energy.

For the total capture cross section we run our code up to $n=25$ (summed over all l and m values) and then make a sum from $n=1$ to 25. These values are presented in Table IV for all three projectiles Ti^{22+}, V^{23+}, and Fe^{26+}. For Fe^{26+} projectiles our total cross section at 500 keV/amu agrees reasonably well with that of Katsonis, Maynard, and Janev [13], while our value is low by a few percent. We expect that contributions from states of $n>25$ will improve our value by a few percent. Results for the projectiles Ti^{22+} and V^{23+} are totally new, to our knowledge.

TABLE IV. Total capture cross sections (cm^2) as a function of energy (keV/amu) by Ti^{22+}, V^{23+}, and Fe^{26+} projectiles. $a\ [-b]$ stands for $a\times 10^{-b}$.

E (keV/amu)	Ti^{22+}	V^{23+}	Fe^{26+}
400	1.428[−16]	2.027[−16]	
500	4.437[−17]	5.967[−17]	5.093[−17]
600	1.776[−17]	2.299[−17]	
700	8.325[−18]	1.046[−17]	1.213[−17]
800	4.371[−18]	5.375[−18]	
900	2.465[−18]	2.973[−18]	3.890[−18]

ACKNOWLEDGMENTS

The authors would like to express their thanks to the International Atomic Energy Agency, Vienna for the encouragement under the research agreement No. 8003/CF. Financial support from the DST, Government of India under the research Grant No. SP/S2/K-01/93 is highly appreciated.

[1] J. Bohdansky, Phys. Scr. **23**, 119 (1981).
[2] R. W. Jensen, D. E. Post, W. H. Grassberger, C. B. Tarter, and W. A. Lokke, Nucl. Fusion **17**, 187 (1977).
[3] E. Hinnov and M. Matioli, Phys. Lett. A **66**, 109 (1978).
[4] D. E. Post, in *Proceedings of the Nagoya Seminar on Atomic Processes in Fusion Plasma, IPPJ-AM-13*, edited by Y. Itikawa and T. Kato (Nagoya University, Nagoya, 1979) p. 38.
[5] H. Ryufuku and T. Watanabe, Phys. Rev. A **18**, 2005 (1978).
[6] H. Ryufuku and T. Watanabe, Phys. Rev. A **19**, 1538 (1979).
[7] H. Ryufuku and T. Watanabe, Phys. Rev. A **20**, 1828 (1979).
[8] J. Eichler, Phys. Rev. A **23**, 498 (1981).
[9] F. T. Chan and J. Eichler, Phys. Rev. Lett. **42**, 58 (1979).
[10] J. Eichler and F. T. Chan, Phys. Rev. A **20**, 104 (1979).
[11] R. K. Janev, D. S. Belkic, and B. H. Bransden, Phys. Rev. A **28**, 1293 (1983).
[12] N. Toshima, Phys. Rev. A **50**, 3940 (1994).
[13] K. Katsonis, G. Maynard, and R. K. Janev, Phys. Scr. **T37**, 80 (1991).
[14] W. Fritsch, Phys. Scr. **T37**, 89 (1991); D. R. Schultz, L. Meng, C. Reinhold, and R. E. Olson, *ibid.* **T37**, 89 (1991).
[15] S. Dutta, C. R. Mandal, S. C. Mukherjee, and N. C. Sil, Phys. Rev. A **26**, 2551 (1982); C. R. Mandal, S. Dutta, and S. C. Mukherjee, *ibid.* **24**, 3044 (1981); **30**, 1104 (1984); G. C. Saha, S. Dutta, and S. C. Mukherjee, *ibid.* **34**, 2809 (1986).
[16] D. S. F. Crothers and K. M. Dunseath, J. Phys. B **20**, 4115 (1987).
[17] N. C. Deb, Phys. Rev. A **38**, 1202 (1988).
[18] K. M. Dunseath, D. S. F. Crothers, and T. Ishihara, J. Phys. B **21**, L461 (1988).
[19] N. C. Deb and D. S. F. Crothers, J. Phys. B **22**, 3725 (1989).
[20] M. J. Caola, J. Phys. A **11**, L23 (1978).
[21] N. C. Deb, N. C. Sil, and P. Mandal, Ind. J. Phys. **68B**, 267 (1994).